สำนักงานวิทยทรัพยากร
จุฬาลงกรณ์มหาวิทยาลัย

CHAPTER III

RESULTS AND DISCUSSION

3.1 Design Concept

As discussed in Chapter 1, a ligand design may start from preorganizing the existing ligating groups on a platform. The platform of choice in this research is calix[4]arene because it imparts hydrophobicity, one requirement for a long live ISE membrane, to a new host. The remain is to find appropriate ligating moieties.

Benzothiazolyl compounds have been known for its capability of forming metal-ligand complexes (Figure 3.1). Nitrogen in benzothiazolyl group can act as a donor atom for transition metals. For example, 2-(*o*-hydroxyphenyl)-benzothiazole

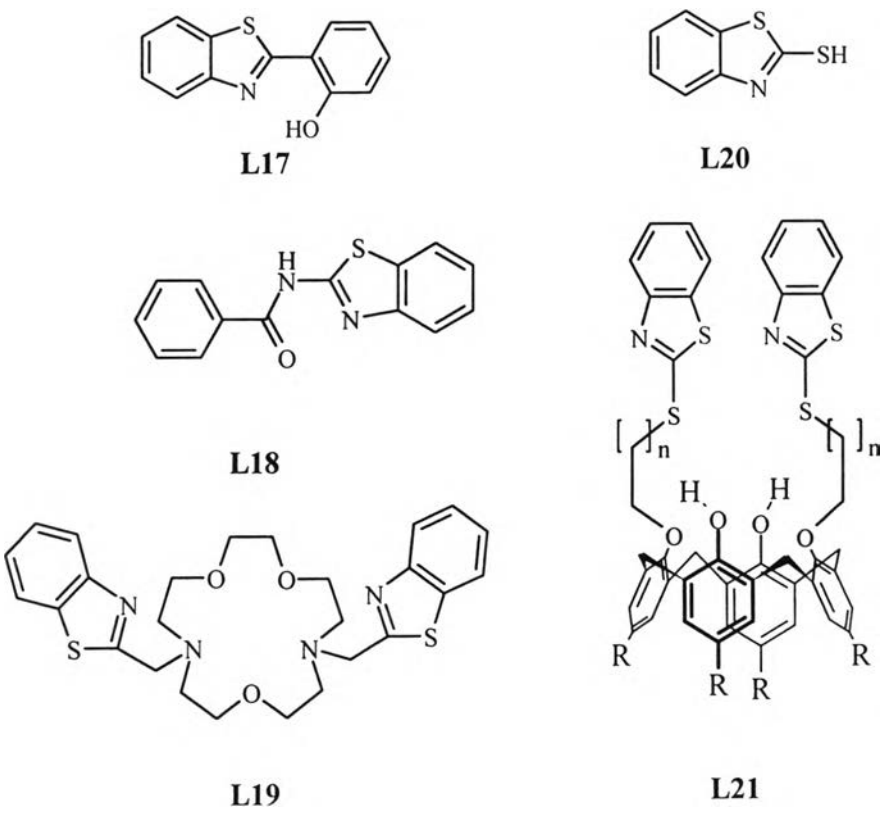

Figure 3.1. Some ligands based on benzothiazolyl group

L17 gave precipitate with Cu^{2+}, Cd^{2+}, Pb^{2+}, Co^{2+}, and Ni^{2+} in acetic-acetate buffer [65]. *N*-benzothiazol-2-yl-benzamide **L18** has been shown to form complexes with

Cu^{2+}, Ni^{2+}, Pd^{2+} and Zn^{2+} upon deprotonation [66]. Benzothiazolyl group attached to diazacrown ether **L19** showed selectivity towards Ag^+ from liquid-membrane transport experiment [67]. A compound 2-mercaptobenzothiazole **L20** has been suggested as a chelating agent for Bi, Cd, Co, Cu, Au, Pb, Hg, Ni, Tl and Zn [68]. When use as the ionophore for mercury ion-selective membrane electrode, it showed selectivity towards mercury with the most serious interference from Ag^+ (log $K^{pot}_{Hg,Ag}$ = -0.70) [69]. When mercaptobenzothiazole were appended on the narrow rim of calix[4]arenes **L21** and used as an ionophore for Ag^+-ISE, the ISE showed the selectivity towards silver ion with good discrimination against Hg^{2+} [70]. Varying tether lengths between benzothiazolyl and calix[4]arene from n = 2 to n = 5 resulted in decreased selectivity of Ag^+ from Na^+ (log $K^{pot}_{Ag,Na}$ decreased from -4.7 to -3.2) but increased selectivity of Ag^+ from Hg^{2+}(log $K^{pot}_{Ag,Hg}$ from -2.5 to -3.2). The alkyl groups on the wider rim of the calix[4]arene skeleton affected of ISE response [70]. Without alkyl substituent (R = H), the response was 58.6 mVdecade^{-1} whereas with *tert*-butyl group the response was only 56.5 mV decade^{-1}. It is postulated that the ionophore bearing *tert*-butyl group on the upper rim must overcome the higher energy barrier in the coordinate adjustment of the two benzothiazolyl groups than that of without *tert*-butyl group. Another possibilities was that the intramolecular inter *tert*-butyl groups might cause some steric hindrance during the coordinate adjustment of the two benzothiazolyl groups. These two possibilities were all favorable for rapid interfacial ion exchange in membrane electrode.

From the consideration above, the benzothiazolyl group was chosen as a ligating group. Another binding point was considered to be O or S in order to provide more coordination points. The chain length between ligating groups and calixarene platform was varied as well as the alkyl group at the wider rim. The proposed structure was shown below.

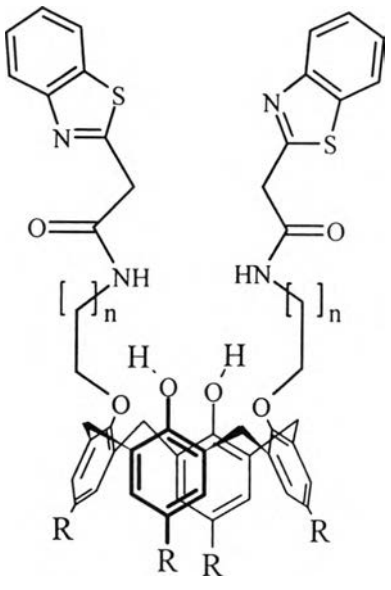

R = H or *tert*-Bu
n = 1 or 3

3.2 Synthesis and Characterization of 5,11,17,23-Tetra-*p*-*tert*-butyl- 25,27-bis(benzothiazolylacetamidobutoxy)calix[4]arene (15)

Synthesis of compound **15** was outlined in Scheme 3.1. The synthesis of compounds **3** and **4** were carried out following the literature procedure [71]. In the first step, calix[4]arene **1** was reacted with 4-bromobutyronitrile in the presence of potassium carbonate in acetonitrile to give a cyano compound **3**. Reduction of **3** with $LiAlH_4$ in diethyl ether produced amino compound **4** which was used immediately for further reaction. The reaction of **4** with ethyl cyanoacetate was modified from Salol procedure [72]. The final step, a condensation of cyanoacetamido compound with 2-aminothiophenol, was done by heating the two reactant together [73] to give the desired product **15**.

The characterization of **15** was carried out by ^{1}H-NMR spectroscopy (Figure A9), elemental analysis (Table 3.1) and mass spectrometry (Figure A10). The results agree with the proposed structure.

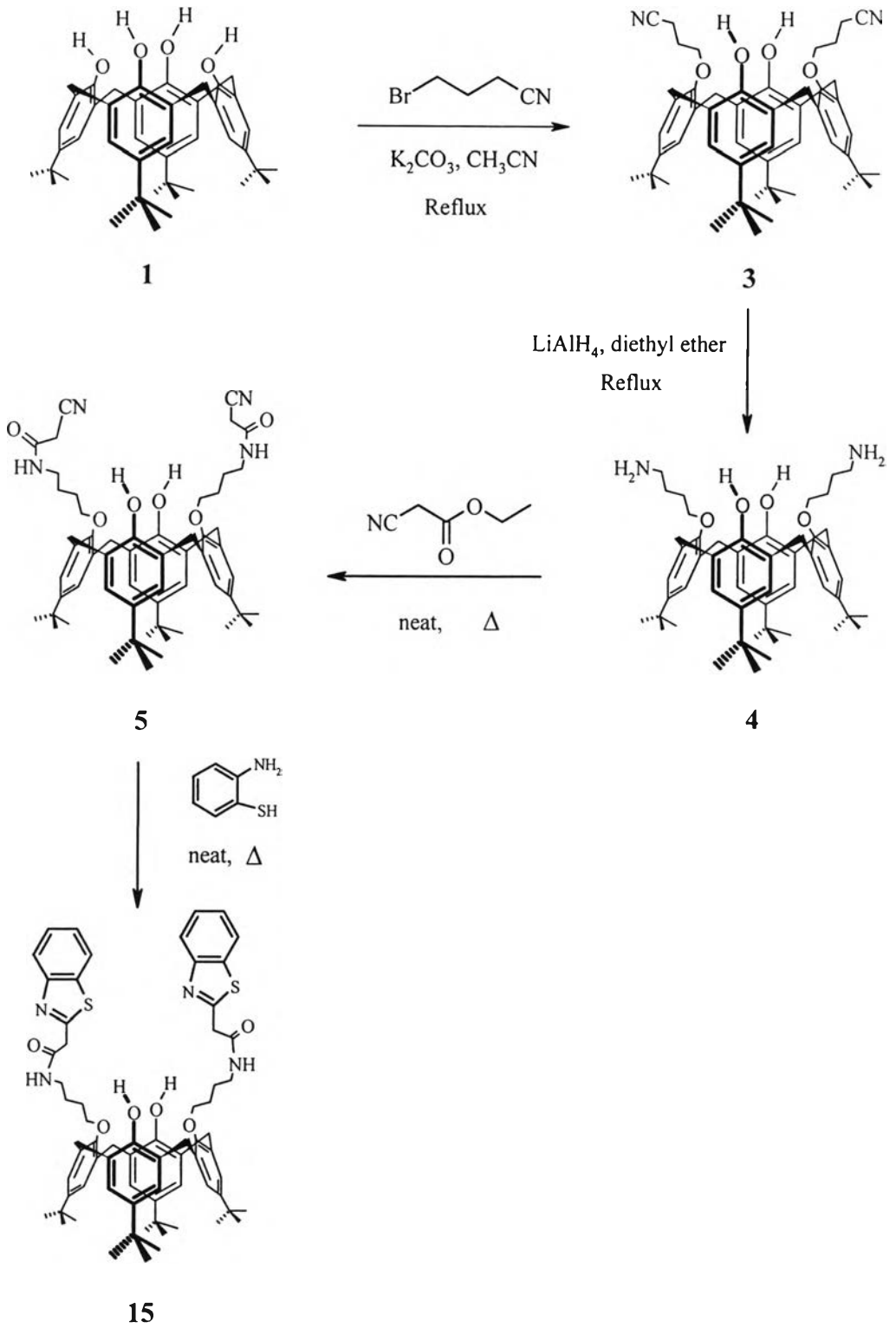

1 **3** **4** **5** **15**

Scheme 3.1 Synthetic pathway of compound **15**

Table 3.1 Elemental analysis data for **15**

	%C	**%H**	**%N**
Calculated	73.65	7.42	4.91
Found	73.68	7.45	4.94

3.3 Synthesis and Characterization of Bis(benzothiazolylacetamidobutoxy) 25,27-dihydroxycalix[4]arene (16)

Synthesis of compound **16** was outlined in Scheme 3.2. The synthesis of compounds **6** was carried out using the same method as for *tert*-butyl analogue (**3**). However, reduction of **6** with $LiAlH_4$ in diethyl ether was inefficient presumably due to low solubility of **6** in diethyl ether. Therefore, the reduction was done in THF as described for a similar cyanoethoxycalix[4]arene [76] to give a corresponding amino compound (**7**). The reaction of **7** with ethyl cyanoacetate was also found to be inefficient. Therefore, another reaction pathway was looked for which ended up with active ester procedure [77]. The procedure consisted of preparing the active ester **19** from cyanoacetic acid with subsequent reaction with amino compound **7** to give the corresponding cyanoacetamido compound **8**. The final step was done as in section 3.2 to give the benzothiazolyl compound **16**.

The characterization of **16** was carried out by ^{1}H-NMR spectroscopy (Figure A11), elemental analysis (Table 3.2) and mass spectrometry (Figure A12). The results agree with the proposed structure.

Table 3.2 Elemental analysis data for **16**

	%C	%H	%N
Calculated	70.72	5.71	6.11
Found	70.73	5.69	6.11

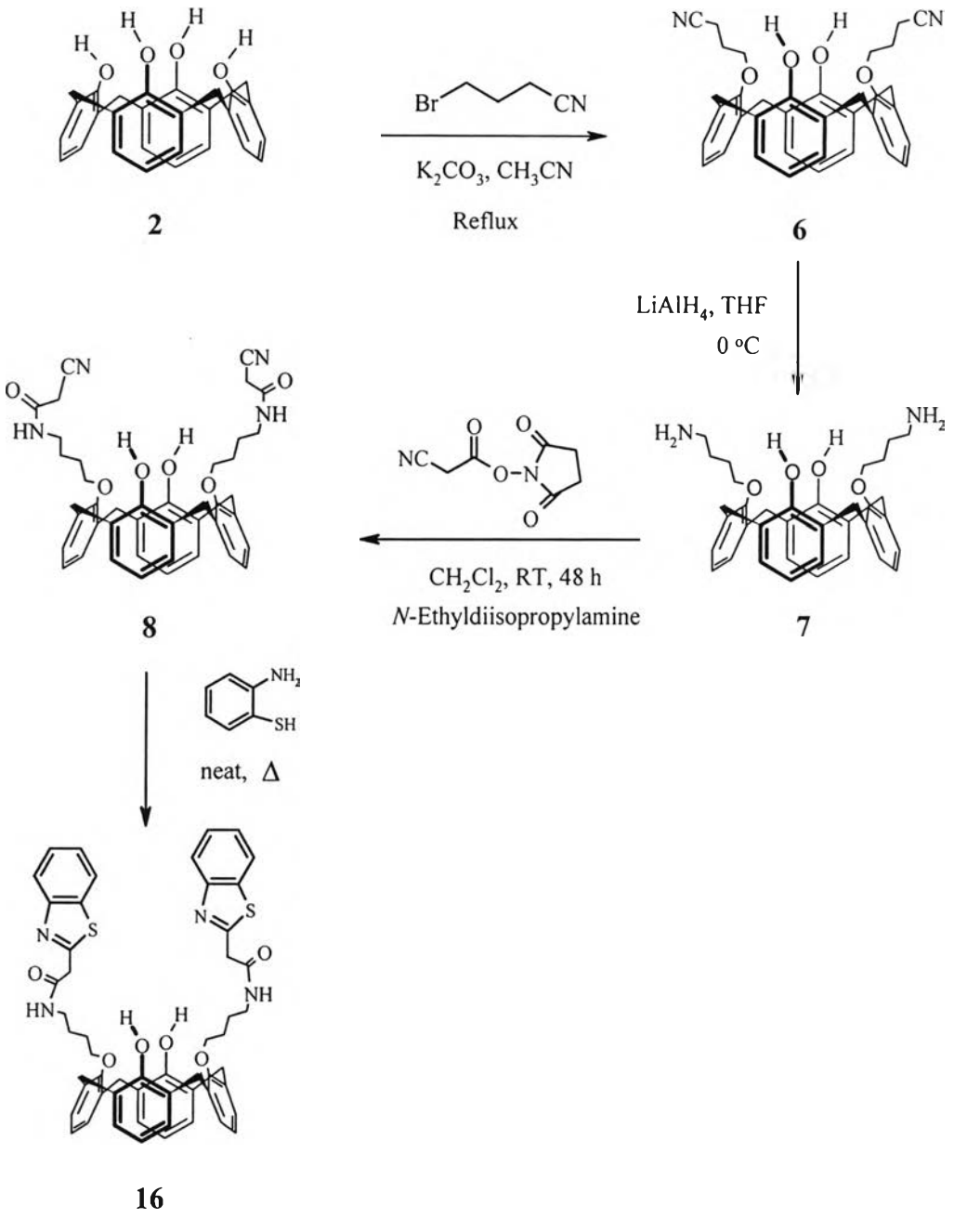

Scheme 3.2 Synthetic pathway of compound **16**

3.4 Synthesis and Characterization of 5,11,17,23-Tetra-*p*-*tert*-butyl-25,27-bis(benzothiazolylacetamidoethoxy)calix[4]arene (17)

Synthesis of compound **17** was outlined in Scheme 3.3. Synthesis of compounds **9** and **10** was carried out as in literature [76]. The remaining steps were as discussed in section 3.2.

The characterization of **17** was carried out by ^{1}H-NMR spectroscopy (Figure A13), elemental analysis (Table 3.3) and mass spectrometry (Figure A14). The results agree with the proposed structure.

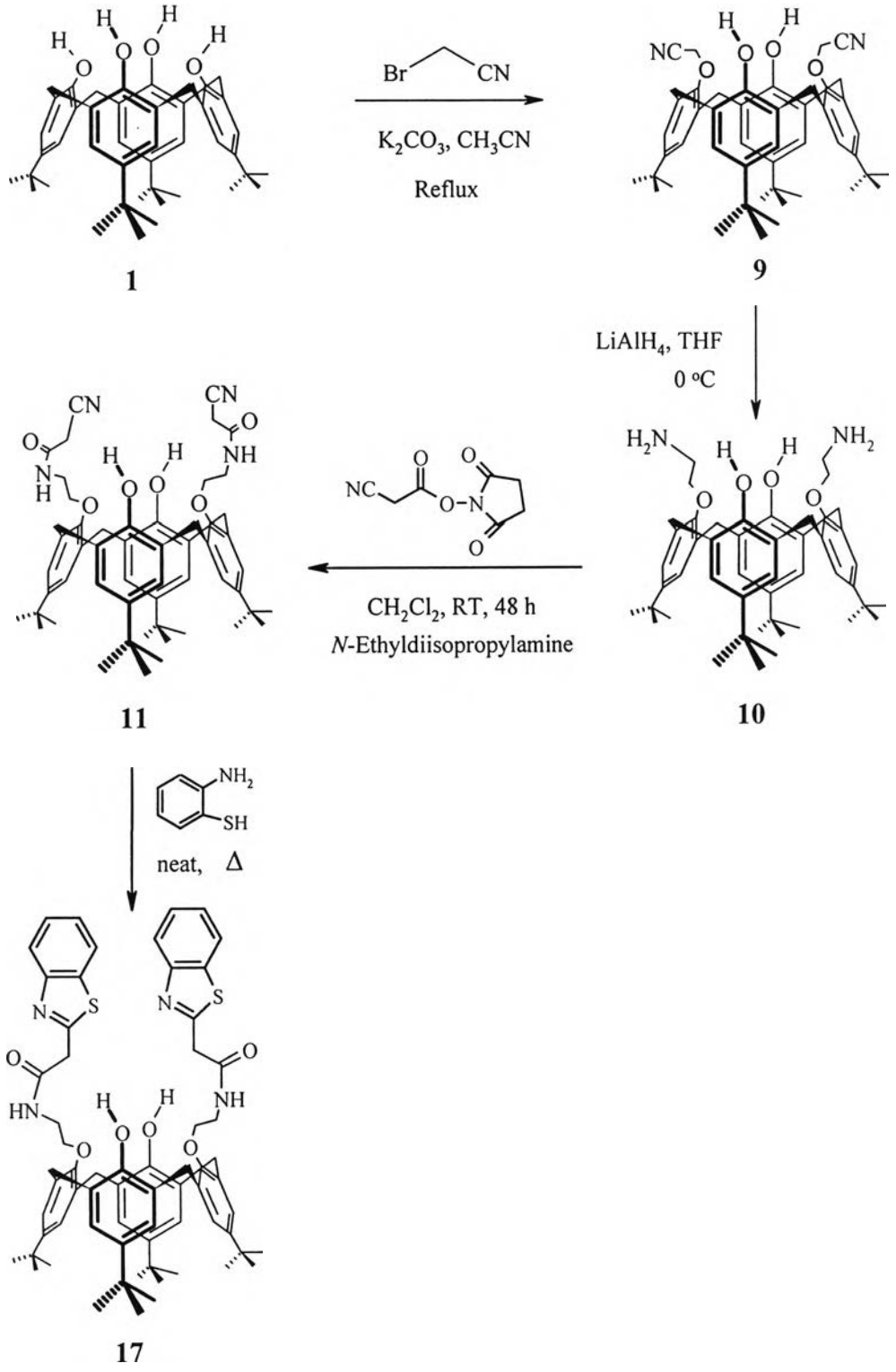

Scheme 3.3 Synthetic pathway of compound **17**

Table 3.3 Elemental analysis data for **17**

	%C	%H	%N
Calculated	73.03	7.06	5.16
Found	73.03	7.08	5.12

3.5 Synthesis and Characterization of 25,27-bis(benzothiazolylacetamidoethoxy) 26,28-dihydroxycalix[4]arene (18)

The synthetic pathway of compounds **18** was similar to that for compound **17** (scheme 3.4).

The characterization of **18** was carried out by ^{1}H-NMR spectroscopy (Figure A15), elemental analysis (Table 3.4) and mass spectrometry (Figure A16). The EA results shows unidentified impurities but the ^{1}H-NMR spectroscopy and mass spectrometry agree with the proposed structure.

Table 3.4 Elemental analysis data for **18**

	%C	%H	%N
Calculated	69.75	5.15	6.51
Found	67.70	5.16	6.05

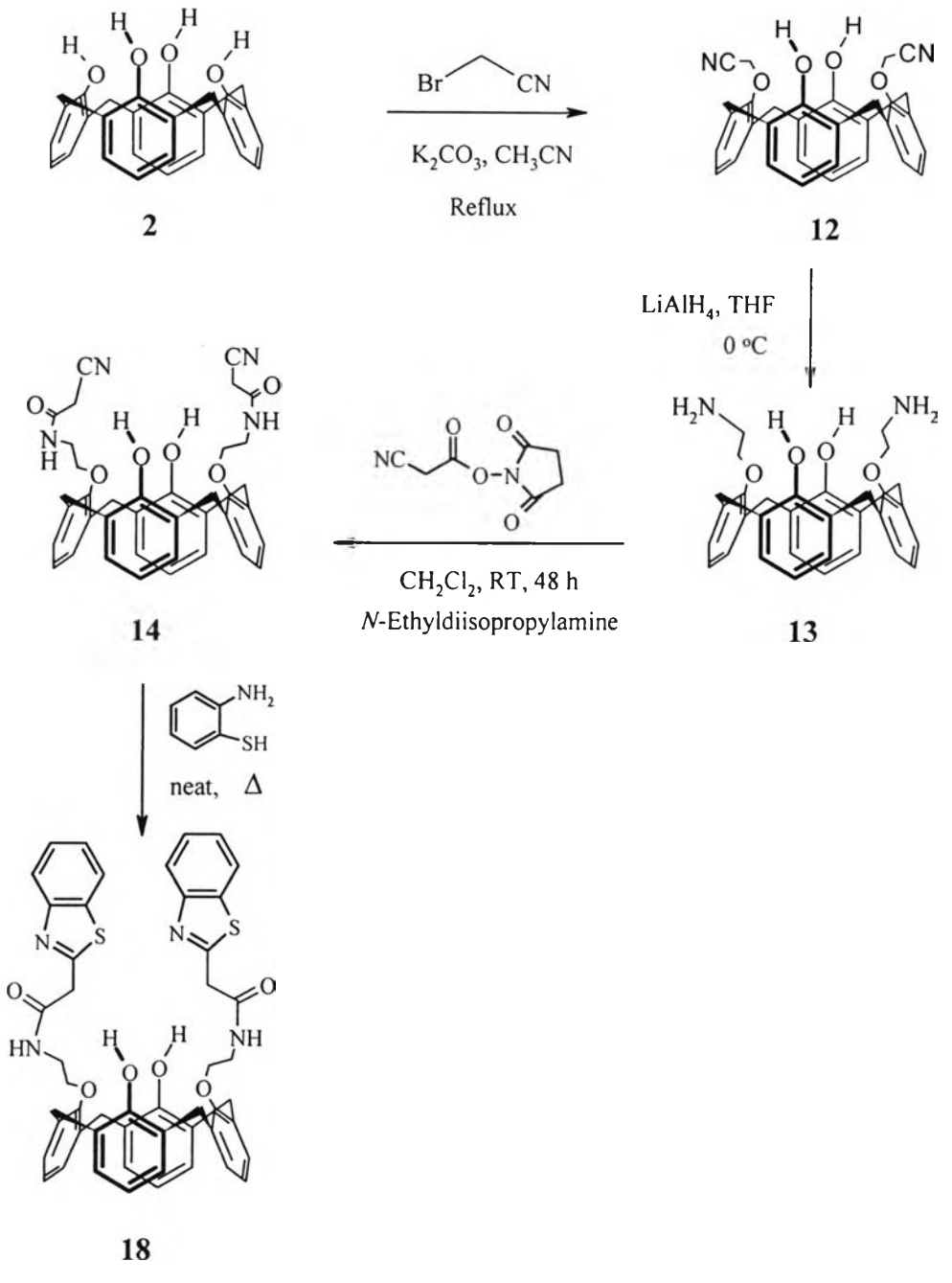

Scheme 3.4 Synthetic pathway of compound **18**

3.6 Cation Complexation Studies

Three common methods to determine the selective property of ionophore are *solvent extraction, liquid-membrane ion-transport measurement* and *determination of stability constant* [78]. The solvent extraction is normally done with a ligand dissolved in chloroform. The aqueous solution of metal is usually prepared from anions of large size such as picrate and perchlorate. It has been known that heavy

metal of these anions are risky from explosion. In transport measurement, the temperature and stirring rate must be precisely controlled to get reproducible results. From these limitations, the determination of stability constant was considered a method of choice to determine the selectivity of the ligands.

3.6.1 Spectral change upon addition of metal ions

Prior to the determination of a stability constant of metal complex using UV-vis spectrophotometric titration, a metal that could change of ligand spectrum should be identified. The metal ions studied are Cu^{2+}, Ni^{2+}, Hg^{2+}, Cd^{2+}, Pb^{2+}, Ca^{2+}, Mg^{2+}, K^{+} and Na^{+}. All ligands (**15-18**) show two peak maxima, one at about 254 nm and another in the range of 270-290 nm. For all ligands, Cu^{2+} and Ni^{2+} cause *bathochromic* shift of the ligand peak at 254 nm and an *isobestic point* is clearly seen (Figure 3.2). These indicate the formation of metal complexes. Addition of Hg^{2+} leads to *hyperchromic effect* at 270-290 nm but the effect on the peak at 254 nm is obscured due to high absorption of the metal which lead to a noise after correction (Figure 3.3). The change of ligand spectra with other metal ions, Cd^{2+}, Pb^{2+}, Ca^{2+}, Mg^{2+}, K^{+} and Na^{+} are small (Figure 3.4). Therefore, only three metal ions were subjected to titration.

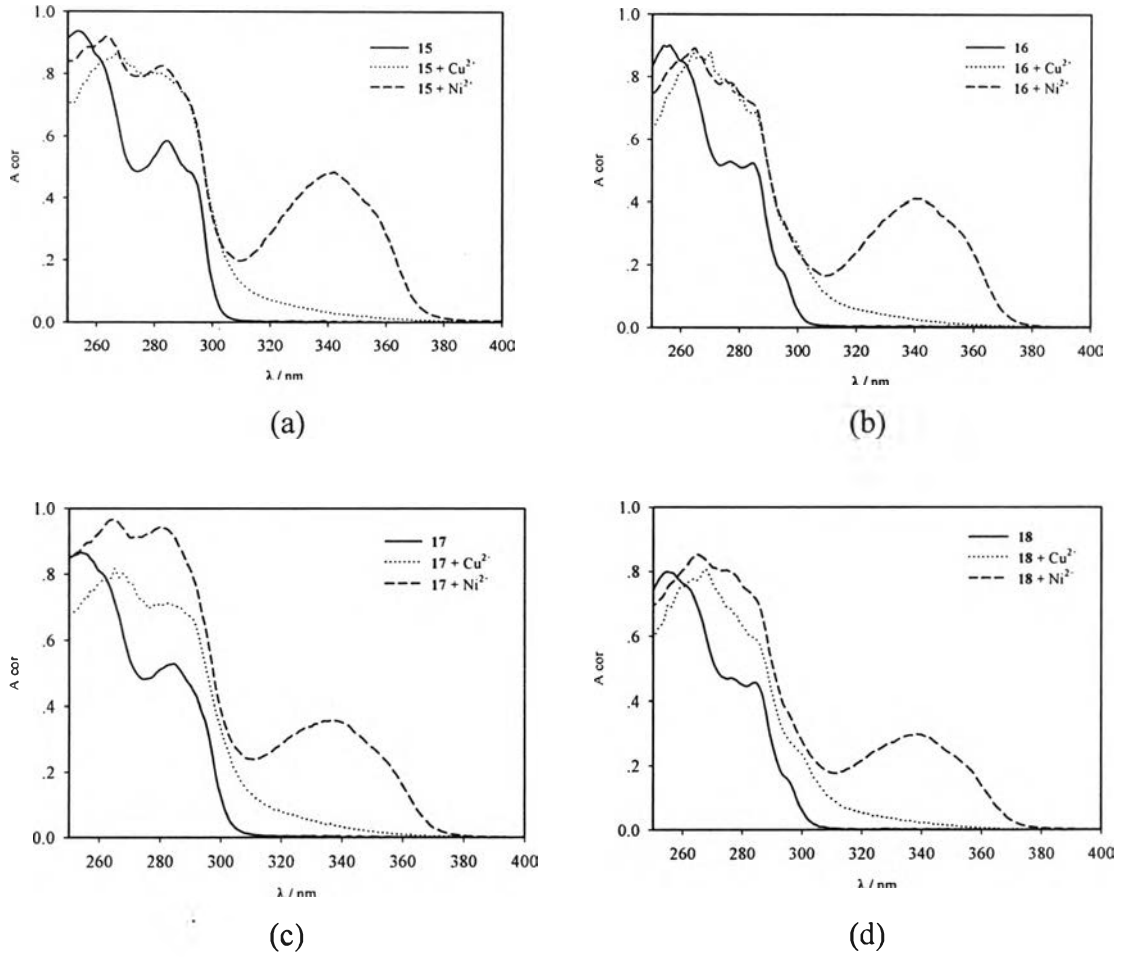

Figure 3.2 A change of ligand spectrum upon addition of Cu^{2+} (5 equiv.) and Ni^{2+}(40 equiv.) to (a) compound **15** (b) compound **16** (c) compound **17** (d) compound **18**. Ligand concentration = 5.0×10^{-5} M in 10%(v/v) acetonitrile-methanol

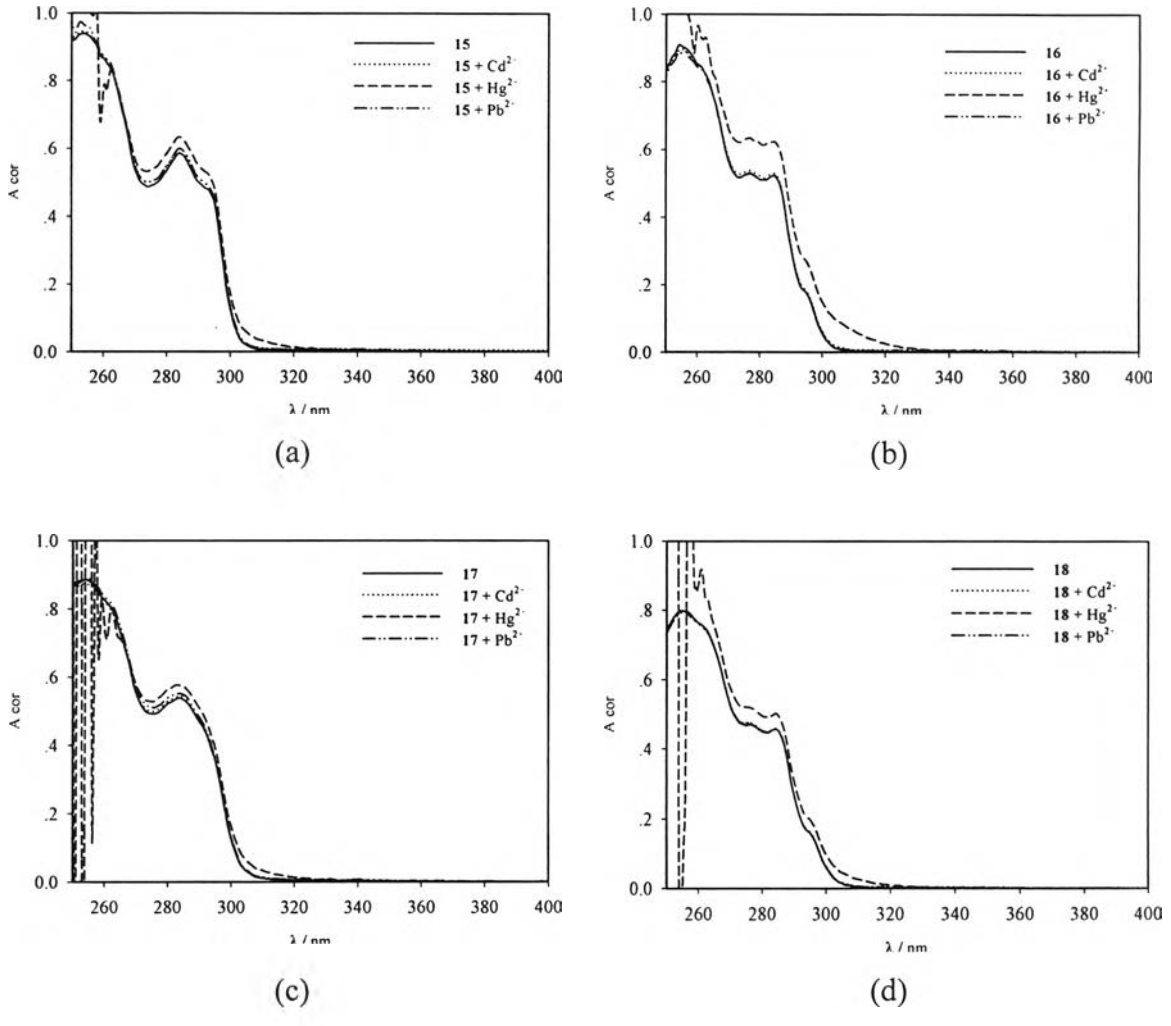

Figure 3.3 A change of ligand spectrum upon addition of Hg^{2+}, Cd^{2+}, Pb^{2+}(40 equiv.) to (a) compound **15** (b) compound **16** (c) compound **17** (d) compound **18**. Ligand concentration = 5.0×10^{-5} M in 10% (v/v) acetonitrile-methanol

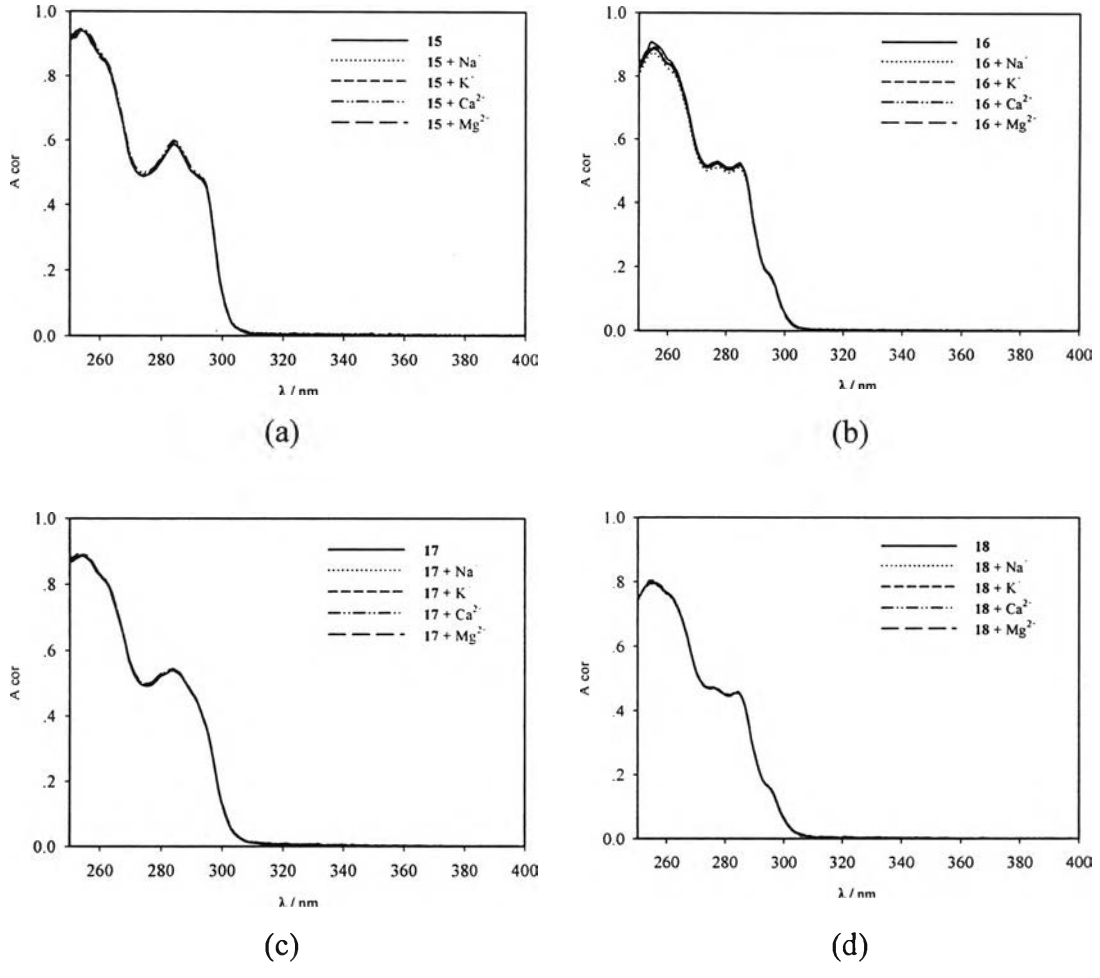

Figure 3.4 A change of ligand spectrum upon addition of Ca^{2+}, Mg^{2+}, K^{+}, Na^{+} (100 equiv.) to (a) compound **15** (b) compound **16** (c) compound **17** (d) compound **18.** Ligand concentration = 5.0×10^{-5} M in 10% (v/v) acetonitrile-methanol

3.6.2 Studies of the ligand spectrum

The peak maxima of the ligand may give a clue to a functional group of the ligand that interact with metal ions. There are three possible chromophores in the ligands: aromatic in *phenolic* group of calix[4]arene, *amide* group and *benzothiazolyl* group. It was known that UV absorption of alkyl group occurs at very short wavelengths which is normally not accessible by typical spectrometer [79]. Therefore, in order to identify the functional group responsible for absorption maxima of the spectra of **15-18**, the amide and benzothiazolyl derivatives of butylamine were synthesized. It was found that *N*-butylcyanoacetamide **20** *shows no absorption in the*

wavelength region under study. Therefore, *amide functional grou*p is not responsible for peak maxima in the spectra of the compounds **15-18**. A similar case is the amide group in peptides and related ligands in which the longest absorption of the amide group occurs near 220 nm and is due to n $\rightarrow \pi^*$ [80]. The spectrum of of 2-(1,3-benzothiazol-2-yl)-*N*-butylacetamide (**21**) was compared with 5,11,17,23-tetra-*p-tert*-butyl-26,28-bis(acetamidobutoxy)calix[4]arene (**5**) (Figure 3.5). It was clear that the peak maximum at 254 nm appears in compound **21** but not compound **5**. This comes to the first conclusion that the *peak maximum at 254 nm is originated from benzothiazolyl functional group*. Another point is that compound **5** shows peak maxima at 270-290 nm while the amide function group would not absorb in this wavelength region. Therefore, peak maxima at 270-290 nm could be assigned to aromatic groups of calix[4]arene. This maxima coincides with the absorption peaks of benzothiazolyl group of compound **21** (Figure 3.5). Therefore, the second conclusion is *both benzothiazolyl group and aromatic ring of calixarene* are responsible to the peak maxima at *270-290* nm of compound **15**.

From these conclusions, the bathochromic shift of ligand spectra at 254 nm due to Cu^{2+} and Ni^{2+} could be attributed to the interaction of the metals with benzothiazolyl group. Although the interaction of metal with other functional groups is not evident from UV spectra, it is likely that the *amide (carbonyl) oxygen* is a dominant point of interaction. This possibility is drawn from a studies of metal ion complexes with peptides in which the metal forms chelate through amide oxygen in neutral solution and with amide nitrogen in basic solution [80].

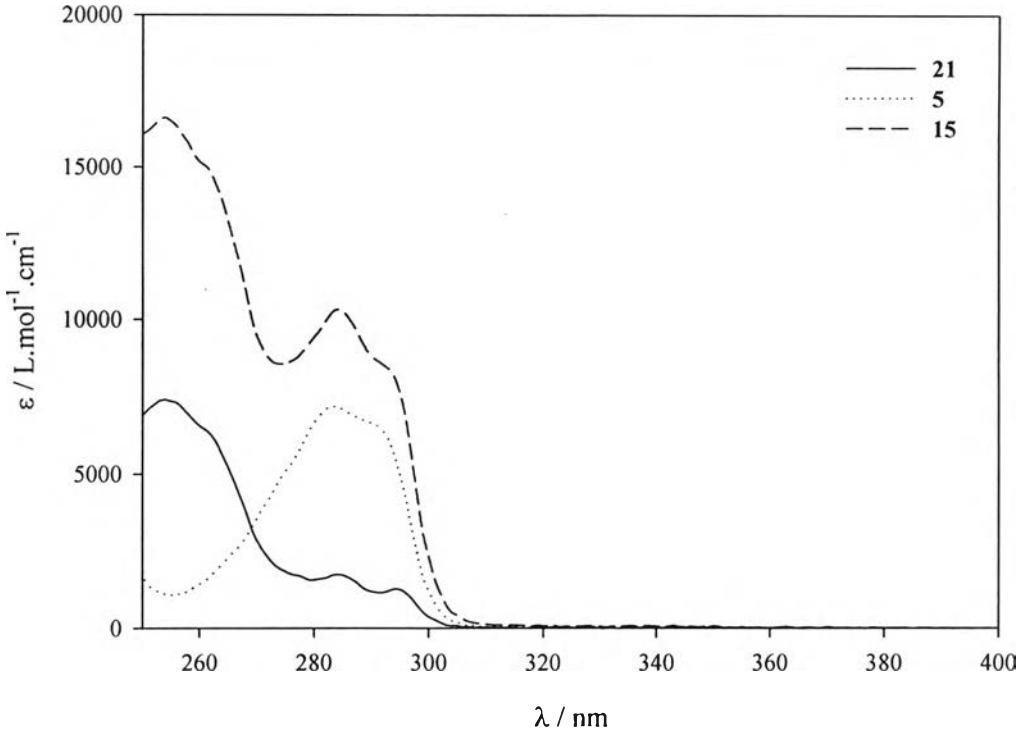

Figure 3.5 A comparison of spectrum of 2-(1,3-benzothiazol-2-yl)-*N*-butylacetamide **(21),** 5,11,17,23-tetra-*p-tert*-butyl-25,27-bis(cyanoacetamido-butoxy)calix[4]arene **(5)**, and 5,11,17,23-tetra-*p-tert*-butyl-25,27-bis(benzothiazolylacetamidobutoxy)calix[4]arene **(15)** in 10% (v/v) acetonitrile-methanol

3.6.3 Determination of stability constant

The stability constant of metal complex (Cu^{2+}, Ni^{2+} and Hg^{2+}) were determined in duplicate by titrating the ligand with about 6 equivalents of metal ion. The calculation with SIRKO showed that the change in spectrum fitted with the model of 1:1 ligand to metal complex. A typical spectrum during titration is shown in Figure 3.6 and the value of stability constants are shown in Table 3.5.

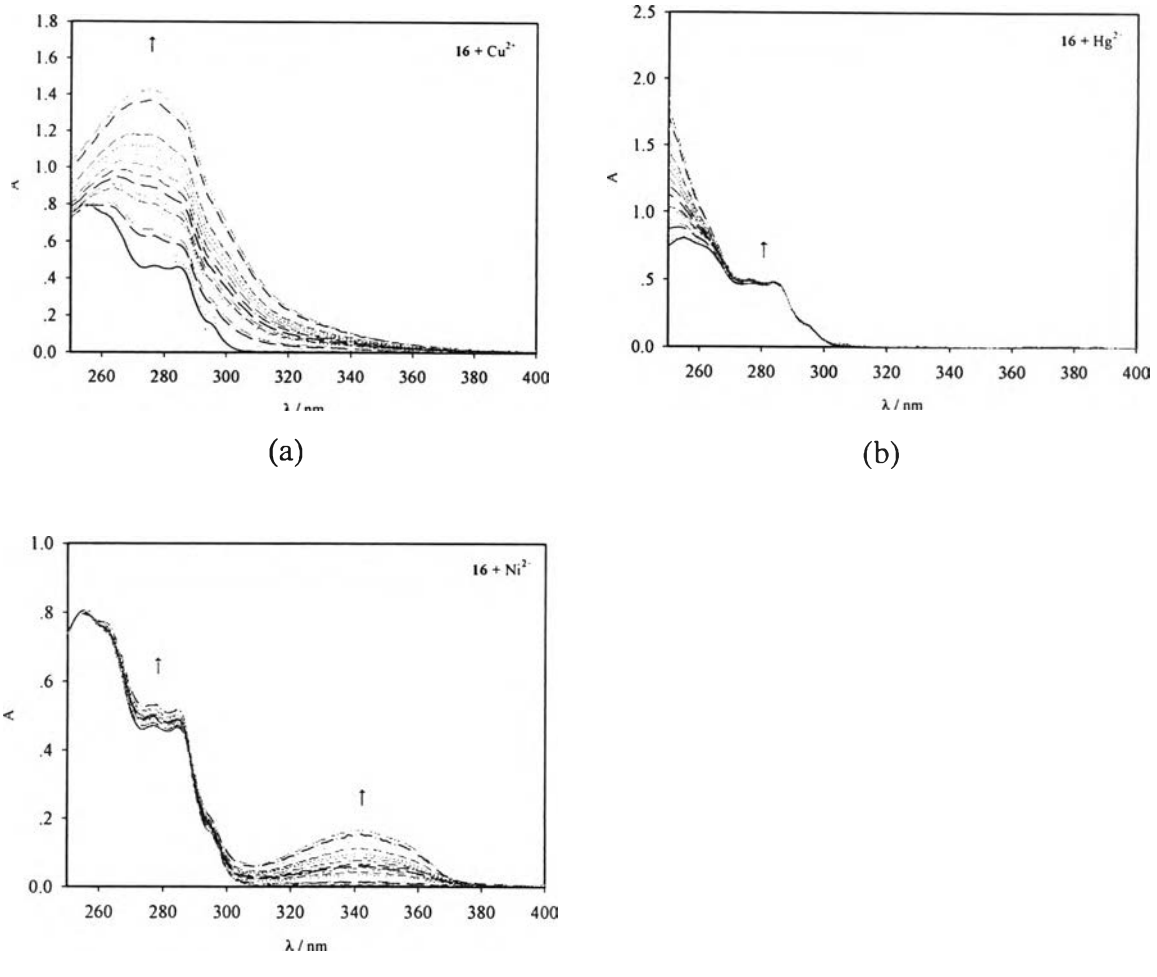

(a) (b)

(c)

Figure 3.6 Typical spectrum change upon titration of compound **16** with (a) Cu^{2+} (b) Hg^{2+} (c) Ni^{2+}. Ligand concentration = 4.9×10^{-5} M; $0 < C_M/C_L < 6$

The selectivity of the compounds can now be predicted on the magnitude of the stability constant: the all compounds are selective toward Cu^{2+} compared with Ni^{2+} but not selective toward Hg^{2+}.

The literature which describes the selectivity through stability constants are sparse [81]. Those available are presented in Table 3.6 [82-83] and the corresponding ligands in Figure 3.7.

Table 3.5 Stability constant of ligand-metal complexes

Ligand	log β (ML)		
	CuL	NiL	HgL
15	3.79	2.40	3.83
	3.78	2.41	3.31
16	3.91	2.25	3.35
	3.91	2.35	3.42
17	4.00	2.79	3.99
	4.08	2.79	3.60
18	3.84	2.71	3.48
	3.86	2.71	3.79

Table 3.6 Some stability constants of calixarene derivatives

Metal ions	log β (ML)	
	L22* [82]	**L23**** [83]
Cu^{2+}	4.3 ± 0.1	4.1
Pb^{2+}	3.8 ± 0.3	-
Eu^{2+}	4.11 ± 0.04	-
Hg^{2+}	-	3.9
Ag^{+}	-	4.4

* in methanol at 25°C; 0.01 M tetraethylammonium chloride

** the condition of titration is not specified

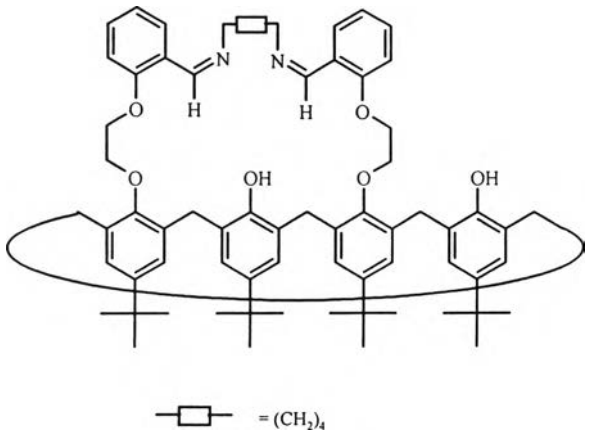

L22[82]

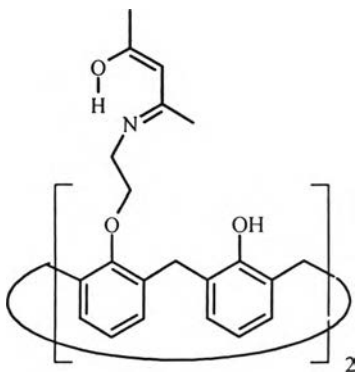

L23 [83]

Figure 3.7 The structure of the ligands in Table 3.6

3.6.4 Determination of stoichiometry of metal complexes [84]

Although the stoichiometry of metal complexes could be found from a model fitting (as in SIRKO), it is customary to verify with other methods such as *mole-ratio plots* and *Job's method.* The principle of the Job's method is that the mole-ratio of the metal ion (concentration C_M) and the ligand (concentration C_L) is varied between 0 and 1 at constant total concentration C_T ($C_T = C_L + C_M$) and the absorbance of the solutions of different composition is measured. The absorbances are then plotted against the mole-fraction of the ligand (x_L). If only one complexes species has been formed, with composition ML_n, the absorbances are measured at the wavelength where neither the metal ion or the ligand but only the complex absorbs, then n can be calculated from the abscissa of the maximum of the curve (x_{max}):

$$n = \frac{x_{max}}{1 - x_{max}} \qquad (17)$$

There are several limitations of the method. One is that if more than one complex is formed simultaneously, as the position of the maximum changes with total concentration C_T chosen, and the equation yields only the average ligand number.

In the experiment, two total concentration were chosen, 5.0×10^{-5} M and 5.0×10^{-4} M and only one ligand **16** was studied. The results of the Job's plot is shown in Figure 3.8. In the Figure, the absorbance at 303 nm was selected as the ligand absorption is low while the Cu^{2+}-complex and Hg^{2+}-complex has a shoulder at this wavelength (See Figure 3.2 and 3.3). The curvature of the plot indicates that x_{max} is about 0.5 in both cases which implies that the stoichiometry of Cu^{2+} and Hg^{2+} with **16** is about 1:1. For Ni^{2+} the peak at 340 nm was not apparent so that the absorbance at 275 nm where the hyperchromic effect is evident was selected. Even so, the plot gives a line with not much curvature so that the x_{max} and stoichiometry of Ni^{2+} complex could not be specified. This unsharpness of the plot was due to the small value of stability constant of Ni complex and the small total concentration [85].

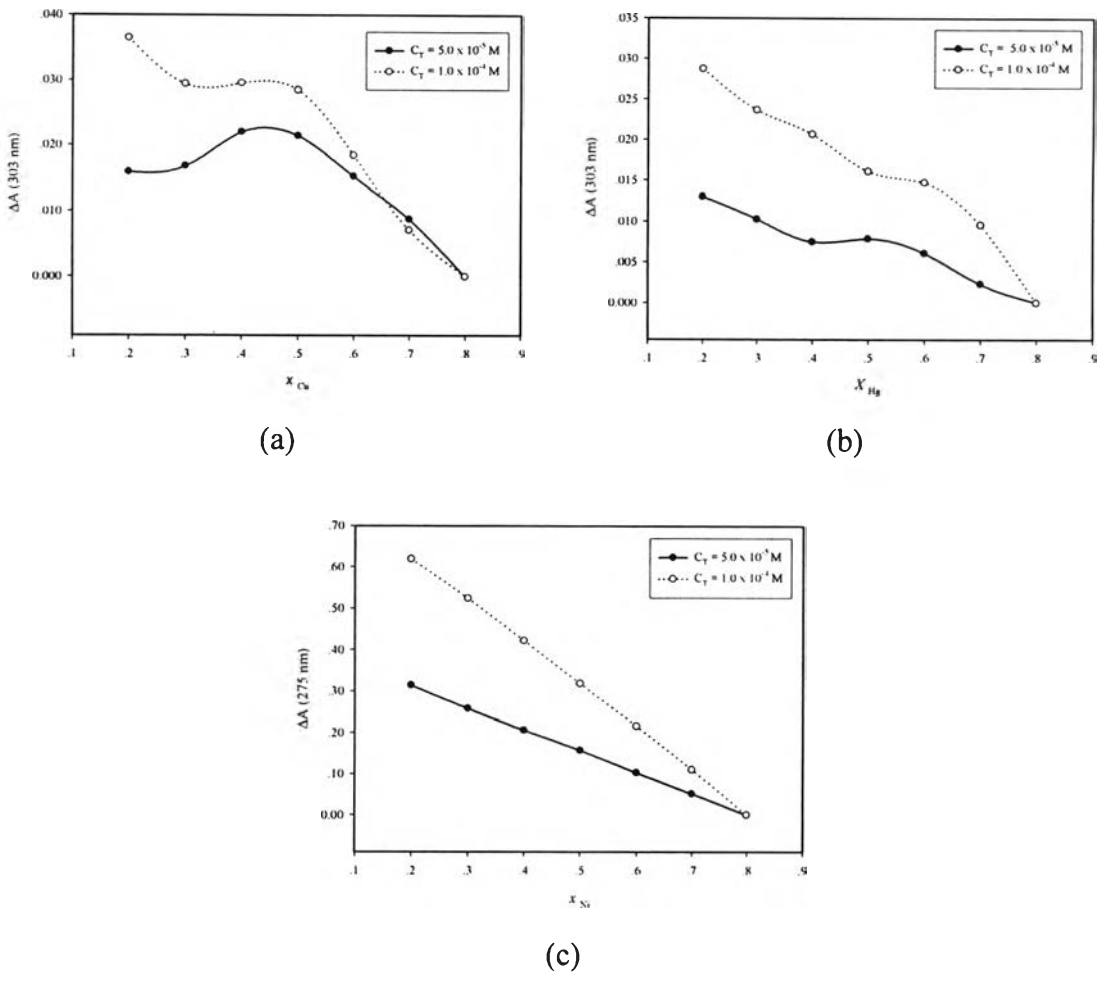

Figure 3.8 The Job's plot of **16** with (a) Cu^{2+}, (b) Hg^{2+} (c) Ni^{2+}

3.7 Ion-Selective Electrode Studies: Potentiometric Selectivity Coefficient of Carrier-Based ISE Based on Compound 15-18, a Preliminary Investigation

Response

The calibration plots of the membranes based on compounds **15-18** were obtained by converting the concentration of Cu^{2+} in each solution into activity using the activity coefficient from the *Debye-Hückel equation* [86] and plotted against measured emf. The plots were shown in Figure 3.9 and the slopes, calculated from a linear regression in the range 10^{-4}-10^{-2} M, are shown in Table 3.7. The **17** and **18**-ISEs show response closer to the theoretical slope (29.5 mV decade^{-1}) than **15** and **16**-ISE. This is probably due to better binding ability of **17**-**18**, with a shorter tether length, in

the *o*-NPOE/membrane [87]. This observation was similar to Ag^+-ISE using benzothiazolylthiaalkoxy-calix[4]arene as an ionophore where the longer tether length gave the lower slope [70].

Potentiometric selectivity

The potentiometric selectivity coefficients of the ISE were determined by the *mixed solution methods*. This method was prefered to the separate solution methods because it closely resembled the real sample where the interfering ions usually coexisted with analyte ions. The FIM was preferred to FPM because it gave the notion of how the interfering ions affected the detection limit from the plots. Note that the FPM involved the addition of interfering ion into the fixed concentration of analyte ion so that the plot of E vs log a_J did not resemble neither a standard calibration curve nor the plot of analyte standard addition.

The variation of emf at varying concentration of Cu^{2+} in interfering ion are shown in Figure 3.10 and the calculated potentiometric selectivity coefficients are shown in Table 3.8. For clarity, the structure of the ligands were shown below the Table. It is apparent that the most serious interference from divalent metal is Pb^{2+}. This might be described from equation (9) in Chapter I that the contribution of the term K_{IJ} may be a dominate factor responsible for $K^{pot}_{Cu^{2+},Pb^{2+}}$ because Pb^{2+} is more lipophilic than Cu^{2+}.

If the ligands do not form complexes with metal ions, the membrane in contact with aqueous solution of metal ions may behave like the organic phase in the solvent extraction where the plasticizer act as an organic solvent. The selectivity of the membrane is expected to follow the lipophilicity of metal ions in the membrane. In technical terms, the selectivities are determined by the difference between the ions in the aqueous and organic phase [7].

A similar behaviour was found in the metal extraction with β-ketoimine calix[4]arene (**L23**, Figure 3.7). While only Ag^+, Cu^{2+} and Hg^{2+} produced change in ligand UV-spectrum so that the stability constants of these metal ions could be determined from UV-vis titration, the extraction studies with the ligand in $CHCl_3$ at pH 4.8 showed that the percent extraction of Cu^{2+} and Hg^{2+} did not exceed 5%. In contrast, Na^+, K^+, Ca^{2+}, Mn^{2+} were extracted with high efficiency at about 40%, 25%, 28% and 15%, respectively. At pH 8 in the presence of pyridine as catalyst, **L23** was

an efficient extractant for Pb^{2+} (86.7%). The reason for this behaviour was not described.

Comparing with recently Cu^{2+}-ISE prepared from porphyrin derivative **L16** (page 21), the selectivity of this ISE toward Cd^{2+} and Ni^{2+} was comparable while that of Ca^{2+} was better. However, the selectivity toward Pb^{2+}, Na^{+} and K^{+} was poorer.

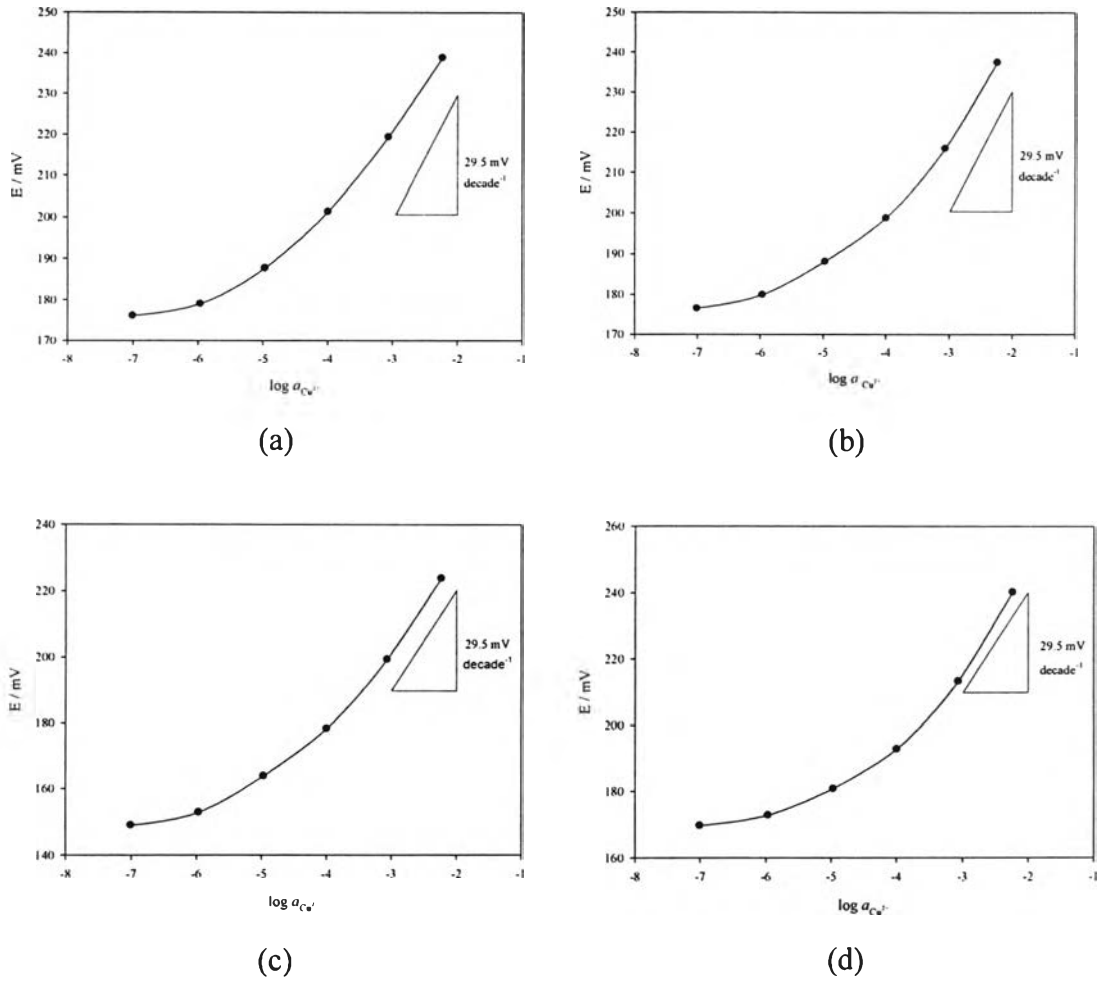

Figure 3.9 The response of ISE electrodes preparation from (a) compound **15** (b) compound **16** (c) compound **17** and (d) compound **18**

Table 3.7 Slope of the calibration plots

	Ionophore			
	15	**16**	**17**	**18**
slope (mV decade^{-1})	21.3	21.9	25.9	26.8
correlation coefficient (r)	0.9985	0.9953	0.9971	0.9936

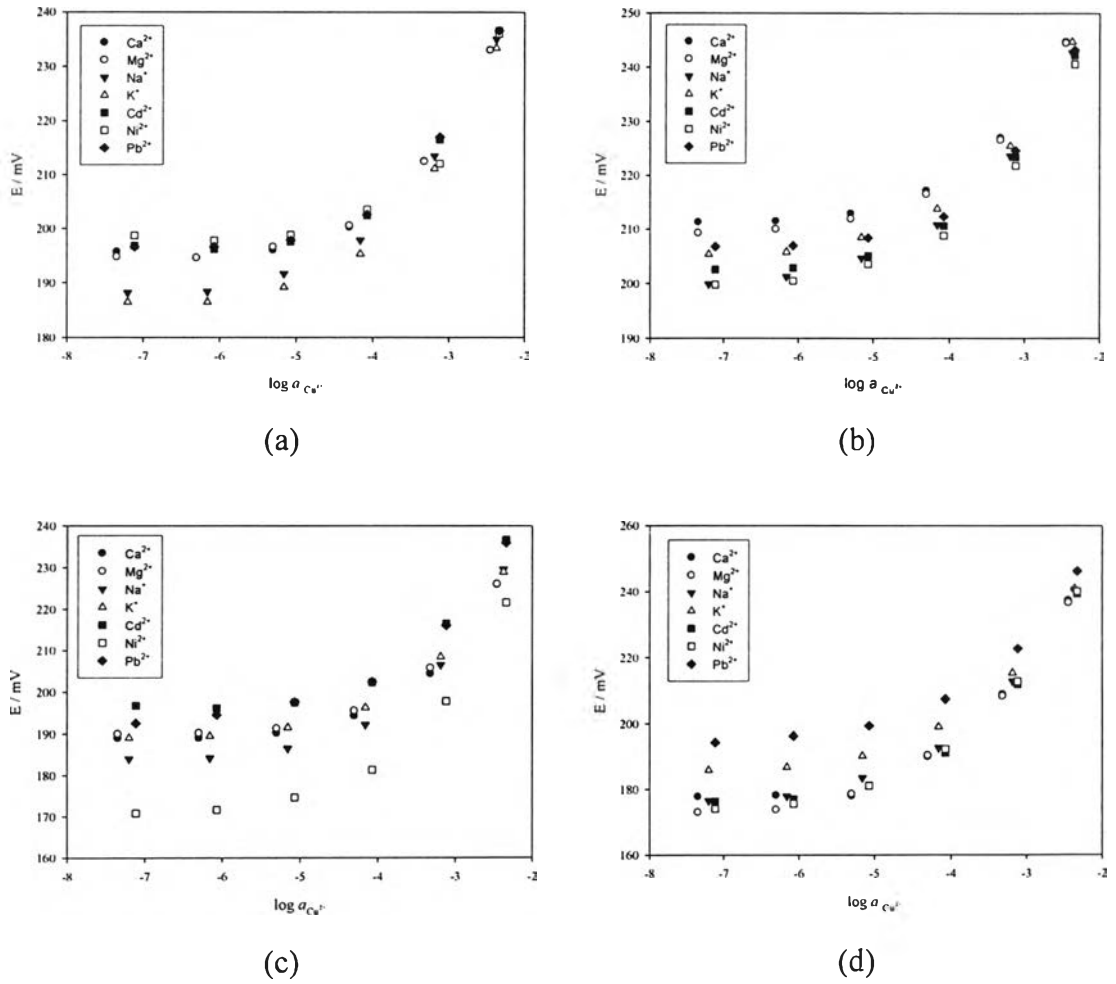

Figure 3.10 The variation of emf at varying concentration of Cu^{2+} in interfering metal ions of ISE from (a) compound **15** (b) compound **16** (c) compound **17** and (d) compound **18**

Table 3.8 The potentiometric selectivity coefficients.

Ion J	$\log K^{pot}_{Cu,J}$			
	15	**16**	**17**	**18**
Cu^{2+}	0	0	0	0
Pb^{2+}	-0.12	-0.27	0.28	-0.07
Cd^{2+}	-1.05	-1.30	-0.95	-1.40
Ni^{2+}	-0.95	-1.30	-1.05	-1.35
Ca^{2+}	-1.84	-1.64	-1.59	-2.29
Mg^{2+}	-1.84	-1.69	-1.59	-2.29
Na^{+}	-0.40	-0.10	0.10	-0.40
K^{+}	-0.30	0.05	0.35	-0.10

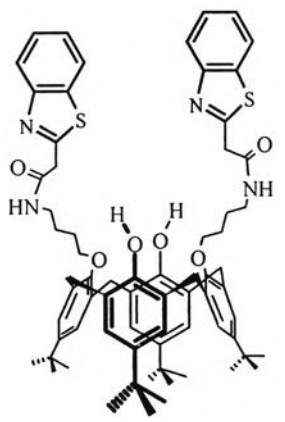

15

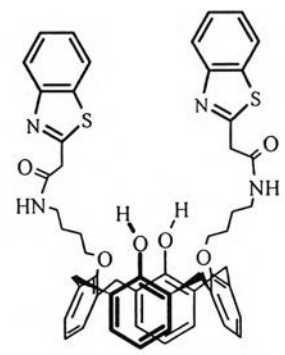

16

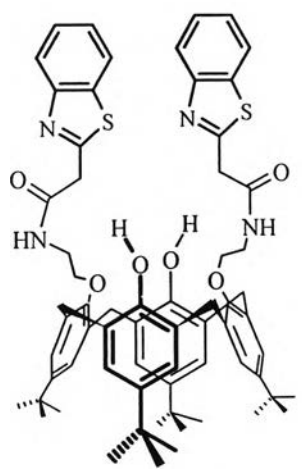

17

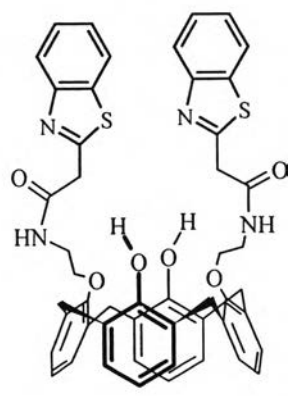

18